NASA Technical Memorandum 4164

Open-Mode Delamination Stress Concentrations in Horseshoe and Elliptic Composite Curved Bars Subjected to End Forces

William L. Ko and Raymond H. Jackson

JANUARY 1990

NASA

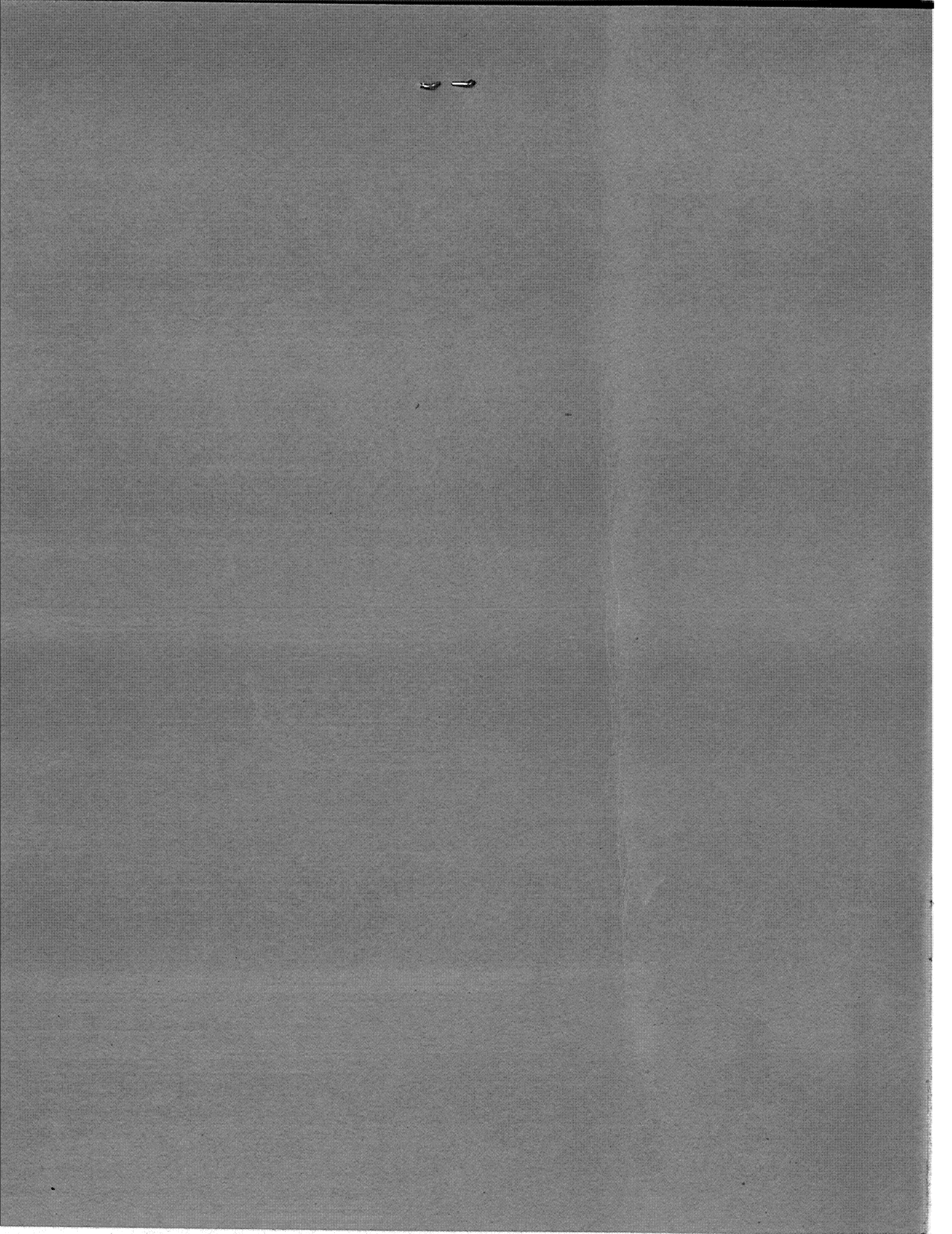

NASA Technical Memorandum 4164

Open-Mode Delamination Stress Concentrations in Horseshoe and Elliptic Composite Curved Bars Subjected to End Forces

William L. Ko and Raymond H. Jackson
Ames Research Center
Dryden Flight Research Facility
Edwards, California

NASA
National Aeronautics and
Space Administration
Office of Management
Scientific and Technical
Information Division

1990

ABSTRACT

The multilayer theory of anisotropic elasticity and a finite element method were used to analyze the open-mode delamination stress concentrations in horseshoe and elliptic laminated composite curved bars. Two types of laminations, solid laminations and sandwich laminations, were analyzed.

It was found that the open-mode delamination stress concentration could be greatly increased in these two types of curved bars by decreasing their aspect ratios. The open-mode delamination stress concentration generated in the solid laminations was found to be far more severe than that generated in the sandwich laminations.

The horseshoe curved bar may be used to determine both the open-mode delamination strength of solidly laminated composites and the open-mode debonding strength of sandwiched laminated composites. However, the elliptic curved bar is only good for determining the open-mode delamination strength of solidly laminated composites.

1 INTRODUCTION

One of the shortcomings of the laminated composite structures is the delaminations between the composite laminas. Once the delaminations take place, the composite structures could lose their structural integrity (that is, stiffness, service life, etc.) and could result in ultimate catastrophic delamination failure. The failure could be either "open-mode" or "shear-mode" delamination failure depending on the stress field induced in the composite structures.

In the applications of the composite materials, certain structural components could contain curved beam regions, or the entire structural components could be in the form of curved panels (either solid laminations or sandwich laminations). When such structural components are subjected to cyclic bendings during service loadings, both radial (thickness direction) and shear stresses could be induced in the structures. These two types of stresses are distributed nonuniformly and their peak values (stress concentration points) are located at different sites where delaminations between composite layers or between face-sheets and sandwich core (debonding) could nucleate. The open-mode delamination can occur only when the bending is in the direction of increasing the curvatures of the curved structural components. However, the shear-mode delamination is invariant to bending directions.

In measuring the open-mode delamination strength of the composite structures, usually a flat square specimen is pulled in the thickness direction (see fig. 1(a)). In this type of test, debonding between the specimen and the load application fixtures (platters) can occur instead of composite delamination. In addition, it is difficult to maintain perfectly parallel separation of the two platters during this type of test. An alternative geometry for the open-mode delamination test specimen is in the shape of a semicircular curved bar shown in figure 1(b). In this type of test specimen, the open-mode delamination can nucleate at the peak tensile radial stress point located at the midspan of the curved bar. Through the use of the theory of anisotropic elasticity, it is possible to calculate the open-mode delamination strength of the composite without direct measurement at the delamination site. The shortcoming of the semicircular curved bar specimen is that under the end forces, the magnitude of the open-mode delamination stress is identical to that of the shear-mode delamination stress (located at either end of the specimen) (ref. 1). Thus, if the composite has weaker delamination strength in shear mode than in open mode, the open-mode delamination cannot be achieved in the semicircular curved bar specimen. The way to circumvent this problem is to generate open-mode delamination stress concentration by changing the specimen geometry to horseshoe shaped or elliptic shaped, etc. This paper presents the studies of the open-mode delamination stress concentrations which could be generated in the said two types of test specimens fabricated with solid laminations or sandwich laminations.

NOMENCLATURE

A, B, D	arbitrary constants associated with nonpure bending
a	inner radius of semicircular region of horseshoe curved bar
a_i	outer radius of ith layer of semicircular region of horseshoe curved bar
a_m	mean radius of semicircular region of horseshoe curved bar, $\frac{1}{2}(a + b)$
B', C', D'	arbitrary constants associated with pure bending
b	outer radius of semicircular region of horseshoe curved bar, or semi-minor axis of outer boundary of elliptic curved bar
c	semi-major axis of outer boundary of elliptic curved bar
E_L	modulus of elasticity of single ply in fiber direction
E_T	modulus of elasticity of single ply transverse to fiber direction
E_r	modulus of elasticity in r direction
E_θ	modulus of elasticity in θ direction
$E41$	quadrilateral membrane element
e	moment arm, $M = Pe$
G_{LT}	shear modulus of single ply
$G_{r\theta}$	shear modulus associated with r–θ system
h	width of semicircular curved bar
i	index associated with ith layer, $i = 1, 2, 3, \ldots, N$
K	open-mode stress concentration factor, $[(\sigma_r)_{max}$ of any curved bar$]/[(\sigma_r)_{max}$ of semicircular curved bar$]$
k	anisotropic parameter, $\sqrt{\frac{E_\theta}{E_r}}$ associated with pure bending
M	applied end moment, $M = Pe$
N	total number of laminated layers
P	applied end force
r	radial distance
r_0	radial location of zero σ_θ
SPAR	structural performance and resizing
t	thickness of curved bar
t_c	sandwich core thickness (or depth)
t_f	thickness of sandwich face sheets
u_r	displacement in r-direction
u_θ	displacement in θ-direction
x, y	rectangular Cartesian coordinates
β	anisotropic parameter, $\sqrt{1 + \frac{E_\theta}{E_r}(1 - 2\nu_{r\theta}) + \frac{E_\theta}{G_{r\theta}}}$ associated with nonpure bending
θ	tangential coordinate
ν_{LT}	Poisson ratio of single ply composite

$\nu_{r\theta}, \nu_{\theta r}$	Poisson ratios associated with r–θ coordinates
ξ	distance in thickness direction measured from inner boundary of elliptic curved bar
σ_r	radial stress
σ_r^*	debonding stress calculated from strength of materials
$(\sigma_r)_{max}$	open-mode delamination stress (maximum tensile radial stress)
σ_r^M	radial stress induced by the end moments M
σ_r^P	radial stress induced by the end forces P
σ_θ	tangential stress
$\tau_{r\theta}$	shear stress
$[\ ]^{(i)}$	quantity associated with ith layer
$[\ ]_i$	quantity associated with ith layer

2 COMPOSITE CURVED BARS

2.1 Horseshoe Curved Bar

Figure 2 shows the geometry of the horseshoe curved bar which consists of a semicircular region and two straight regions at both ends. This type of curved bar specimen could be ideal for testing the open-mode delamination strength of the solidly laminated composites or sandwich laminated composites.

By properly adjusting the end moment arm e (the length of the end straight region), it is possible to increase the intensity of the peak radial stress several times that of the peak shear stress. Thus, the open-mode delamination failure can be achieved (instead of delamination failure in shear).

The bending of the horseshoe curved bar under end forces P can be analyzed by the superposition of the following two cases shown in figure 3 (for small deformations):

1. Semicircular curved bar subjected to end forces P (nonpure bending),
2. semicircular curved bar subjected to end moments $M = Pe$ (pure bending).

By using the multilayer theory developed by Ko (ref. 2) for the pure and nonpure bendings of a laminated semicircular composite curved bar (solid or sandwich laminations), it is possible to calculate the open-mode delamination stress in terms of the applied load (measured) without direct measurement (which is nearly impossible) of the delamination stress at the delamination nucleation site. In the analysis the thicknesses of the two composite face sheets of the sandwich lamination will be set equal (see fig. 2). The open-mode delamination stress will be calculated for different aspect ratios of the horseshoe curved bar for studying the effect of the aspect ration on the delamination stress concentration.

2.2 Elliptic Curved Bar

The second type of curved bar (candidate geometry for the open-mode delamination test specimen) analyzed was a semielliptic curved bar shown in figure 4. The outer boundary of this curved bar is semielliptic, but the inner boundary is not elliptic due to constant thickness. No attempt was made to develop a multilayer theory for this type of curved bar. Instead, a finite element method was used to analyze the open-mode delamination stress concentration in this type of curved bar (solid and sandwich laminations) for different curved bar aspect ratios for comparison with the case of horseshoe curved bar.

3 MULTILAYER THEORY

The multilayer theory developed by Ko (ref. 2) (using Lekhnitskii's anisotropic stress functions (ref. 3)) for a laminated anisotropic semicircular curved bar under pure or nonpure bending may be used to calculate the open-mode delamination stress for the horseshoe curved bar. If the semicircular curved bar is fabricated with N number of anisotropic lamina, the stresses and the displacements induced in the ith layer ($i = 1, 2, 3, \ldots, N$) can be written as follows (ref. 2).

3.1 Stresses

a. For end forces P

$$\sigma_r^{(i)}(r,\theta) = \left[A_i\beta_i r^{\beta_i-1} - B_i\beta_i r^{-\beta_i-1} + \frac{D_i}{r}\right]\sin\theta \tag{1}$$

$$\sigma_\theta^{(i)}(r,\theta) = \left[A_i\beta_i(1+\beta_i) r^{\beta_i-1} - B_i\beta_i(1-\beta_i) r^{-\beta_i-1} + \frac{D_i}{r}\right]\sin\theta \tag{2}$$

$$\tau_{r\theta}^{(i)}(r,\theta) = -\left[A_i\beta_i r^{\beta_i-1} - B_i\beta_i r^{-\beta_i-1} + \frac{D_i}{r}\right]\cos\theta \tag{3}$$

b. For end moments M

$$\sigma_r^{(i)}(r) = 2B_i' + C_i'(1+k_i) r^{k_i-1} + D_i'(1-k_i) r^{-k_i-1} \tag{4}$$

$$\sigma_\theta^{(i)}(r) = 2B_i' + C_i'k_i(1+k_i) r^{k_i-1} - D_i'k_i(1-k_i) r^{-k_i-1} \tag{5}$$

$$\tau_{r\theta}^{(i)} = 0 \tag{6}$$

where A_i, B_i, D_i and B_i', C_i', D_i' are two sets of unknown arbitrary constants (associated with the ith layer) which are determined from boundary conditions shown in section 3. Notice that the magnitudes of $\sigma_r^{(i)}$ (eq. (1)) and $\tau_{r\theta}^{(i)}$ (eq. (3)) for the case of end forces P are identical, but are out of phase in the θ direction by $\frac{\pi}{2}$.

3.2 Displacements

a. For end forces P

$$u_r^{(i)}(r,\theta) = \left\{A_i r^{\beta_i}\left[\frac{1}{E_r^{(i)}} - (1+\beta_i)\frac{\nu_{\theta r}^{(i)}}{E_\theta^{(i)}}\right] + B_i r^{-\beta_i}\left[\frac{1}{E_r^{(i)}} - (1-\beta_i)\frac{\nu_{\theta r}^{(i)}}{E_\theta^{(i)}}\right] + D_i(\ln r)\left(\frac{1}{E_r^{(i)}} - \frac{\nu_{\theta r}^{(i)}}{E_\theta}\right)\right\}\sin\theta \tag{7}$$

$$u_\theta^{(i)}(r,\theta) = \left\{A_i r^{\beta_i}\left[\frac{1}{E_r^{(i)}} - \beta_i(1+\beta_i)\frac{1}{E_\theta^{(i)}} - \frac{\nu_{\theta r}^{(i)}}{E_\theta^{(i)}}\right] + B_i r^{-\beta_i}\left[\frac{1}{E_r^{(i)}} + \beta_i(1-\beta_i)\frac{1}{E_\theta^{(i)}} - \frac{\nu_{\theta r}^{(i)}}{E_\theta^{(i)}}\right] + D_i\left[(\ln r)\left(\frac{1}{E_r^{(i)}} - \frac{\nu_{\theta r}^{(i)}}{E_\theta^{(i)}}\right) - \left(\frac{1}{E_\theta^{(i)}} - \frac{\nu_{\theta r}^{(i)}}{E_\theta^{(i)}}\right)\right]\right\}\cos\theta \tag{8}$$

b. For end moments M

$$u_r^{(i)}(r) = B_i'\left[2r\left(\frac{1}{E_r^{(i)}} - \frac{\nu_{\theta r}^{(i)}}{E_\theta^{(i)}}\right)\right] + C_i'\left[(1+k_i)r^{k_i}\left(\frac{1}{k_i E_r^{(i)}} - \frac{\nu_{\theta r}^{(i)}}{E_\theta^{(i)}}\right)\right] - D_i'\left[(1-k_i)r^{-k_i}\left(\frac{1}{k_i E_r^{(i)}} + \frac{\nu_{\theta r}^{(i)}}{E_\theta^{(i)}}\right)\right] \tag{9}$$

$$u_\theta^{(i)}(r,\theta) = B_i'\left[2r\left(\frac{1}{E_\theta^{(i)}} - \frac{1}{E_r^{(i)}}\right)\right]\theta \tag{10}$$

where the rigid body motion terms are neglected.

3.3 Determinations of Arbitrary Constants

To determine $3N$ unknown constants A_i, B_i, D_i or B_i', C_i', D_i' $(i = 1,2,3,\ldots,N)$, $3N$ boundary conditions are required. Those boundary conditions are listed in the following.

a. For end forces P

The traction-free conditions at the inner boundary $(r = a)$ and at the outer boundary $(r = b)$ give two conditions:

$$\sigma_r^{(1)}(a,\theta) = 0 \tag{11}$$

$$\sigma_r^{(N)}(b,\theta) = 0 \tag{12}$$

And the continuities of radial stress σ_r, radial displacement u_r and tangential displacement u_θ at each interface between layer i and $i+1$ $(i = 1,2,3,\ldots,N-1)$ for perfect bonding give $3(N-1)$ conditions:

$$\sigma_r^{(i)}(a_i,\theta) = \sigma_r^{(i+1)}(a_i,\theta) \tag{13}$$

$$u_r^{(i)}(a_i,\theta) = u_r^{(i+1)}(a_i,\theta) \tag{14}$$

$$u_\theta^{(i)}(a_i,\theta) = u_\theta^{(i+1)}(a_i,\theta) \tag{15}$$

Notice that in the traction-free conditions at the free surfaces, and in the stress continuity conditions at each interface, the shear stress $\tau_{r\theta}$ was not included because it has identical r-dependency as σ_r (see eqs. (1) and (3)). Lastly, the expression of the applied force P in terms of the shear stress $\tau_{r\theta}$ at the end $(\theta = 0)$ of the curved bar gives one condition:

$$-P = \sum_{i=1}^{N}\int_{a_{i-1}}^{a_i} \tau_{r\theta}^{(i)}(r,0)\,dr \tag{16}$$

Equations (11) through (16) will give $3N$ conditions for the determination of $3N$ unknown constants A_i, B_i, D_i by solving $3N \times 3N$ simultaneous equations numerically.

b. For end moments M

Similarly the traction-free conditions and the interface stress and displacements continuity conditions give the following $3N-1$ conditions:

$$\sigma_r^{(1)}(a) = 0 \tag{17}$$

$$\sigma_r^{(N)}(b) = 0 \tag{18}$$

$$\sigma_r^{(i)}(a_i) = \sigma_r^{(i+1)}(a_i) \tag{19}$$

$$u_r^{(i)}(a_i) = u_r^{(i+1)}(a_i) \tag{20}$$

$$u_\theta^{(i)}(a_i) = u_\theta^{(i+1)}(a_i) \tag{21}$$

The relationship between the applied moment M and the tangential stress σ_θ gives the Nth condition:

$$-M = \sum_{i=1}^{N} \int_{a_{i-1}}^{a_i} (r - r_0)\sigma_\theta(r)\,dr \tag{22}$$

for the determination of $3N$ unknown constants B_i', C_i', D_i' by solving $3N \times 3N$ simultaneous equations numerically. The r_0 appearing in equation (22) is the unknown radial location where σ_θ is zero. For pure bending the integration of the r_0 term vanishes.

3.4 Superposition of Solutions

The two stress fields calculated for the semicircular curved bar under end forces P (nonpure bending) and end moments M (pure bending), may be superimposed to generate a stress field for the horseshoe curved bar (see fig. 3). The open-mode delamination stress $(\sigma_r)_{max}$ (located on the x-axis, fig. 2) will then be the maximum value of the summation of two radial stresses $\sigma_r^P(r_D, \frac{\pi}{2})$ due to P and $\sigma_r^M(r_D)$ due to M

$$(\sigma_r)_{max} \equiv \sigma_r^P\left(r_D, \frac{\pi}{2}\right) + \sigma_r^M(r_D) \tag{23}$$

where r_D is the radial location of $(\sigma_r)_{max}$, and is determined from the condition $\frac{\partial \sigma_r}{\partial r} = 0$ which gives

$$A_i\beta_i(\beta_i - 1)r_D^{\beta_i} + B_i\beta_i(\beta_i + 1)r_D^{-\beta_i} - D_i + (k_i^2 - 1)(C_i'r_D^{k_i} + D_i'r_D^{-k_i}) = 0 \tag{24}$$

assuming $(\sigma_r)_{max}$ occurs in the ith layer.

4 FINITE ELEMENT ANALYSIS

Finite element stress analysis was performed on the multilayered elliptic curved bar (see fig. 4) by using the structural performance and resizing (SPAR) finite element computer program (ref. 4). Figure 5 shows the SPAR finite element model set up for the elliptic curved bar (solid lamination or sandwich lamination). Because of symmetry with respect to the x-axis, only half span of the curved bar was modeled. The elliptic curved bar was modeled with 22 layers of anisotropic quadrilateral membrane E41 elements in the thickness direction, and 90 E41 elements in the circumferential direction. For the case of sandwich lamination, each of the face sheets was modeled with 5 layers of E41 elements in the thickness direction, and the sandwich core with 12 layers of E41 elements in the thickness direction. The points in the midspan (along x-axis) were allowed to move freely only in the x-direction. This is represented in figure 5 by a train of rollers. At the upper end of the model, only one point lying in the middle surface was constrained in such a way that it could move freely only in the y-direction. This is shown in figure 5 with only one roller. Thus, the end of the model is allowed to rotate freely.

5 NUMERICAL EXAMPLES

The type of composite used in the analysis has the following ply material properties

$$\begin{aligned}
E_L &= 17.2369 \times 10^{10}\,\text{N/m}^2 (25 \times 10^6\,\text{lb/in}^2) \\
E_T &= 0.8274 \times 10^{10}\,\text{N/m}^2 (1.2 \times 10^6\,\text{lb/in}^2) \\
G_{LT} &= 0.4137 \times 10^{10}\,\text{N/m}^2 (0.6 \times 10^6\,\text{lb/in}^2) \\
\nu_{LT} &= 0.33 \\
\nu_{TL} &= 0.01584
\end{aligned}$$

which give the values of anisotropic parameters as $\beta = 7.9272$ and $k = 4.5644$.

The honeycomb core used in the sandwich laminates has the following material properties

$$E_r = 6.8948 \times 10^8 \text{N/m}^2 (0.1 \times 10^6 \text{lb/in}^2)$$
$$E_\theta = 6.8948 \times 10^4 \text{N/m}^2 (10 \text{ lb/in}^2)$$
$$G_{r\theta} = 1.2411 \times 10^8 \text{N/m}^2 (0.018 \times 10^6 \text{lb/in}^2)$$
$$\nu_{\theta r} = 6.5 \times 10^{-5}$$

The semi-minor axes b of both solid and sandwich laminations for the two curved bar geometries (see figs. 2 and 4) were set to be $b = 5.08$ cm (2 in.), but the semi-major axes c of both types of laminates were allowed to change for different aspect ratios.

All the solid laminations were fabricated with 22 layers of 0°-plies (fibers in the circumferential direction), having the total thickness of $t = 0.3175$ cm (0.125 in.). All the sandwich laminations have the total thickness of $t = 1.1608$ cm (0.457 in.), with a sandwich core thickness of $t_c = 0.6350$ cm (0.25 in.), and a face sheet thickness of $t_f = 0.2629$ cm (0.1035 in.). Each of the face sheets contains 18 layers of 0°-plies. This type of sandwich lamination was used in the fabrication of X-wing helicopter rotor blades. For a special case of aspect ratio $b/c = 1$ (that is, a semicircular sandwich curved bar), a sandwich core of $\pm 15°$ lamination was also studied. This type of core has the anisotropic parameters of $\beta = 4.2498$, $k = 2.4304$.

6 RESULTS

6.1 Solid Laminations

Figure 6 shows the distributions of tensile radial stress σ_r along the x-axis for different values of aspect ratio b/c of the horseshoe curved bar with solid lamination. The open-mode delamination stress $(\sigma_r)_{max}$ (maximum value of σ_r) could be increased many times that of the semicircular case ($\frac{b}{c} = 1$) by lowering the aspect ratio b/c of the curved bar. For example, the open-mode delamination stress concentration factor K ($(\sigma_r)_{max}$ of any $\frac{b}{c}$ value normalized by $(\sigma_r)_{max}$ of semicircular case ($\frac{b}{c} = 1$)) for $\frac{b}{c} = 0.1$ reached as high as 14.4431 (for the anisotropic case). Notice that as the value of b/c decreases, the location of $(\sigma_r)_{max}$ point migrates toward the inner boundary of the curved bar. In figure 6, the stress curves for the isotropic case ($\beta = 2$, $k = 1$) were also shown for comparison. The difference between the anisotropic and isotropic cases became more conspicuous for lower aspect ratios $\frac{b}{c} < 0.2$. The isotropic case gave slightly higher value of $(\sigma_r)_{max}$. Figure 7 shows the plots of σ_r along with the x-axis for different values of b/c of the elliptic curved bar fabricated with solid lamination. For the elliptic curved bar, the rate of the increase of K with the decrease of b/c is faster than that of the horseshoe curved bar (see fig. 8). The reason is that for the same aspect ratio b/c, the former has smaller midspan radius of curvature than that of the latter. Notice from figure 8 that the value of K given by elliptic curved bar at $\frac{b}{c} = 0.3$ is slightly higher than that given by the horseshoe curved bar at $\frac{b}{c} = 0.1$ (for the anisotropic case).

6.2 Sandwich Laminations

Figure 9 shows the distributions of σ_r along the x-axis for various aspect ratios of the horseshoe sandwich curved bar. Unlike the case of solid lamination (see fig. 6), $(\sigma_r)_{max}$ occurred in the inner face sheet for the aspect ratios $\frac{b}{c} > 0.3$. For $\frac{b}{c} < 0.2$, the location of $(\sigma_r)_{max}$ moved to the interface between the inner face sheet and the sandwich core. For testing the debonding strength of the sandwich laminations, the aspect ratio $\frac{b}{c}$ of the horseshoe sandwich curved bar test specimen should be designed for $\frac{b}{c} < 0.2$.

Figure 10 presents the distributions of σ_r along the x-axis for different values of b/c of the elliptic sandwich curved bar. For this case, $(\sigma_r)_{max}$ is located within the inner face sheet for the whole range of aspect ratios. Thus the elliptic curved bar specimen is not recommended for testing the debonding strength of the sandwich lamination because the interfacial debonding failure between the face sheet and the sandwich core may not occur if the interlaminar delamination strength of the face sheet is weak and the specimen could fail under interlaminar delamination of the inner face sheet. Again the stress distributions in the sandwich core for all aspect ratios are nearly linear. Figure 11 shows the comparison of the rate of increase of $(\sigma_r)_{max}$ with the decrease in b/c for the horseshoe and elliptic sandwich curved bars. The magnitude of $(\sigma_r)_{max}$ for the sandwich laminations is somewhat lower than that of the solid laminations (see fig. 8). At $\frac{b}{c} = 0.4$, the elliptic case gave the value of $(\sigma_r)_{max}$ as being slightly higher than that given by the horseshoe case at $\frac{b}{c} = 0.1$.

6.3 Semicircular Sandwiches

As presented in section 6.2, for honeycomb core sandwich laminations, $(\sigma_r)_{max}$ never occurred within the honeycomb core. The study of the semicircular sandwich curved bar is to show how the core material properties will affect the location of $(\sigma_r)_{max}$. Figure 12 shows σ_r distribution in the $\theta = \frac{\pi}{2}$ plane for three cases of sandwich core of the semicircular sandwich curved bar under end forces P (nonpure bending). For the honeycomb core (solid curve), the $(\sigma_r)_{max}$ is located in the inner face sheet. As the core material becomes stiffer ($\pm 15°$-lamination, long–short broken curve), the $(\sigma_r)_{max}$ location migrates into the core. The curve for solid lamination is also shown for comparison. Figure 13 shows the case of pure bending of the semicircular sandwich curved bar. Like the nonpure bending, the stiffer core of $\pm 15°$-lamination caused the location of $(\sigma_r)_{max}$ to move within the core (long–short broken curve). For the honeycomb core (solid curve), $(\sigma_r)_{max}$ is always located at the interface between the inner face sheet and honeycomb core. The debonding stress σ_r^* calculated from the strength-of-materials equation (see fig. 14)

$$\sigma_r^* = \frac{M}{hta}$$

is also shown for comparison. The value of σ_r^* is slightly lower than $(\sigma_r)_{max}$ calculated from the multilayer theory (solid curve) and finite element method (solid dots).

7 CONCLUDING REMARKS

The multilayer theory of anisotropic elasticity and a finite element method were used to analyze the open-mode delamination stress concentrations in horseshoe and elliptic laminated composite curved bars of different aspect ratios. Both the solid laminations and sandwich laminations were analyzed. The open-mode delamination stress concentration can be greatly increased in these two types of curved bars by decreasing their aspect ratios. The open-mode delamination stress concentration generated in the solid lamination was more severe than that generated in the sandwich lamination having the same aspect ratio. The elliptic curved bar was slightly more efficient in generating the open-mode delamination stress concentration as compared with the horseshoe curved bar. The horseshoe curved bar could be used for the determination of both the open-mode delamination strength of laminated composites and the debonding strength of the sandwiched composites. The elliptic curved bar is not suitable for determining the debonding strength of the sandwich composites. The location of the open-mode delamination stress is a function of the curved bar geometry and the material properties.

Ames Research Center
Dryden Flight Research Facility
National Aeronautics and Space Administration
Edwards, California, September 26, 1989

REFERENCES

1. Ko, W.L., *Delamination Stresses in Semicircular Laminated Composite Bars*, NASA TM-4026, 1988.

2. Ko, W.L., and R.H. Jackson, "Multilayer Theory for Delamination Analysis of a Composite Curved Bar Subjected to End Forces and End Moments," presented at the Fifth International Conference on Composite Structures, Paisley, Scotland, July 24–26, 1989, NASA TM-4139, 1989.

3. Lekhnitskii, S.G., *Anisotropic Plates*, Gordon and Breach Science Publishers, New York, 1968.

4. Whetstone, W.D., *SPAR Structural Analysis System Reference Manual*, System Level 13A, Vol. 1, Program Execution, NASA CR-158970-1, 1978.

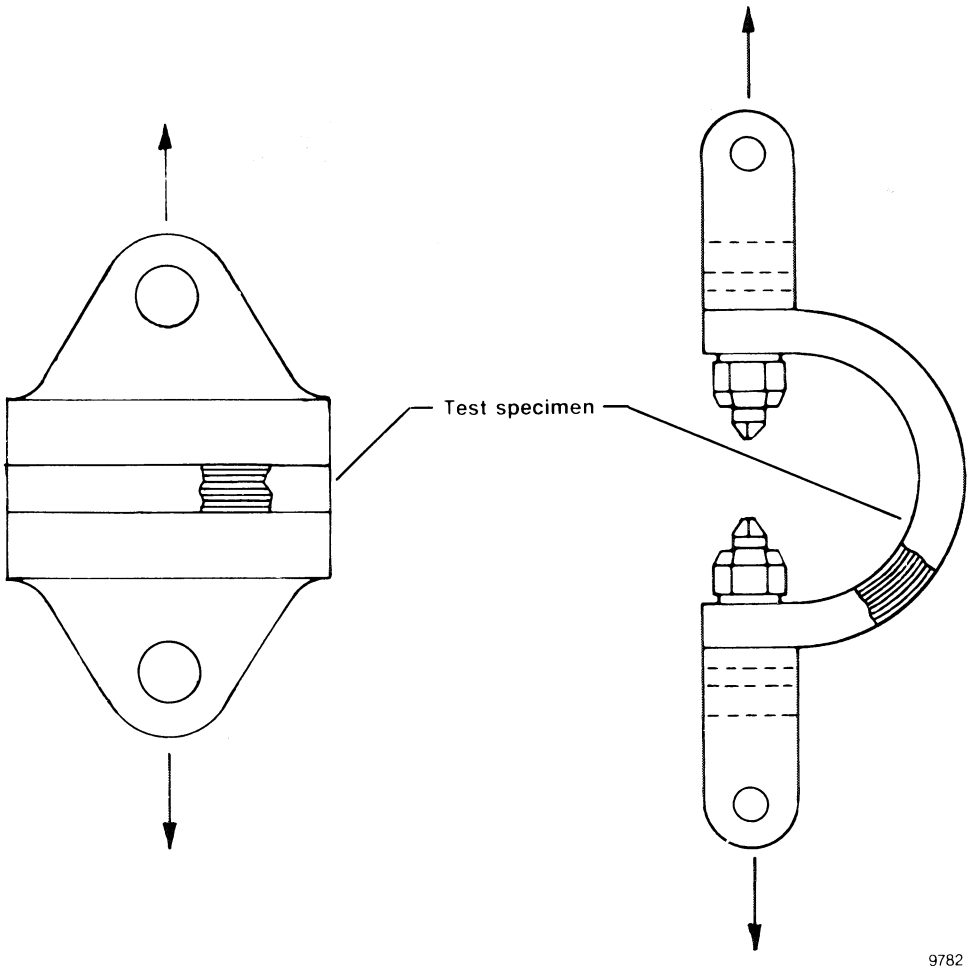

Figure 1. Geometries of composite delamination test specimens.

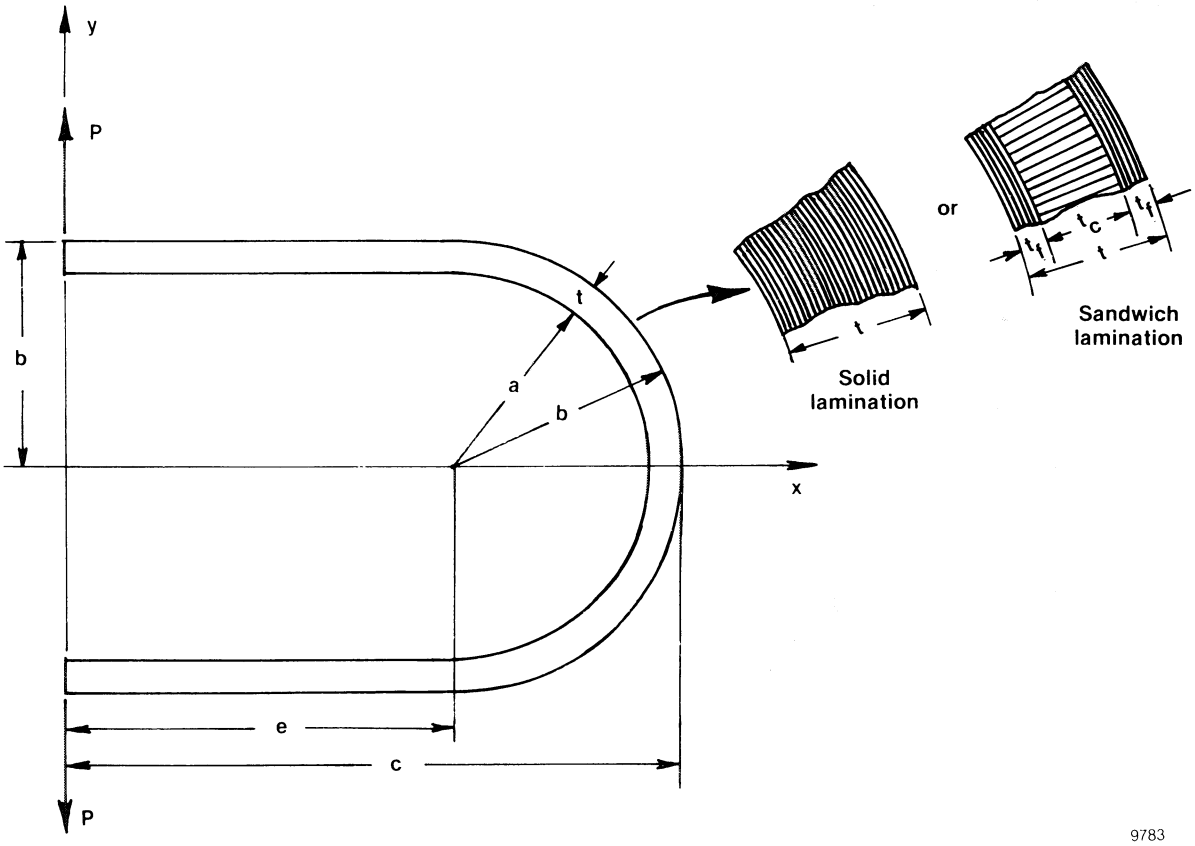

Figure 2. Horseshoe curved bar under end forces.

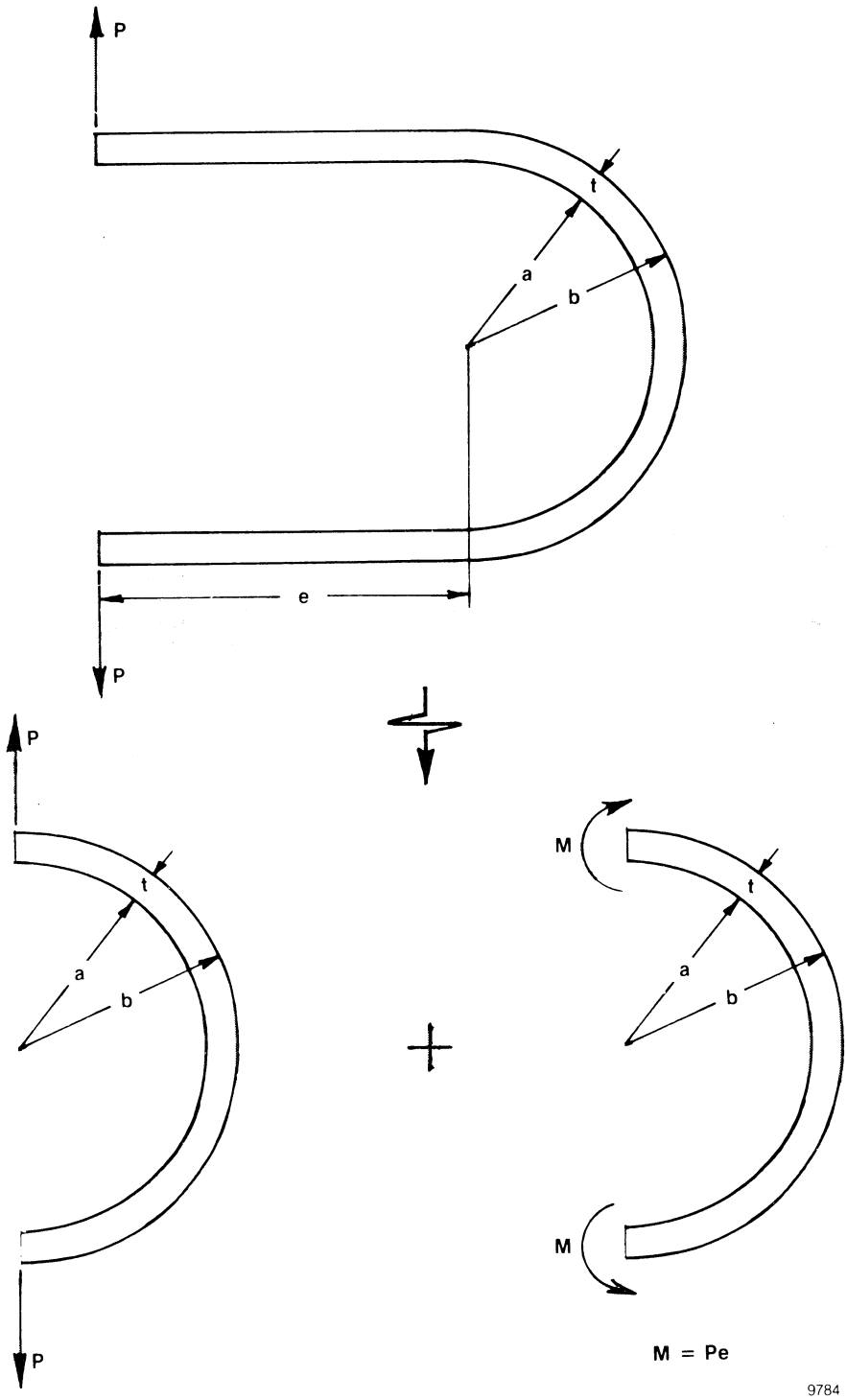

Figure 3. Bending of horseshoe curved bar represented by superposition of pure and nonpure bendings of semicircular curved bars.

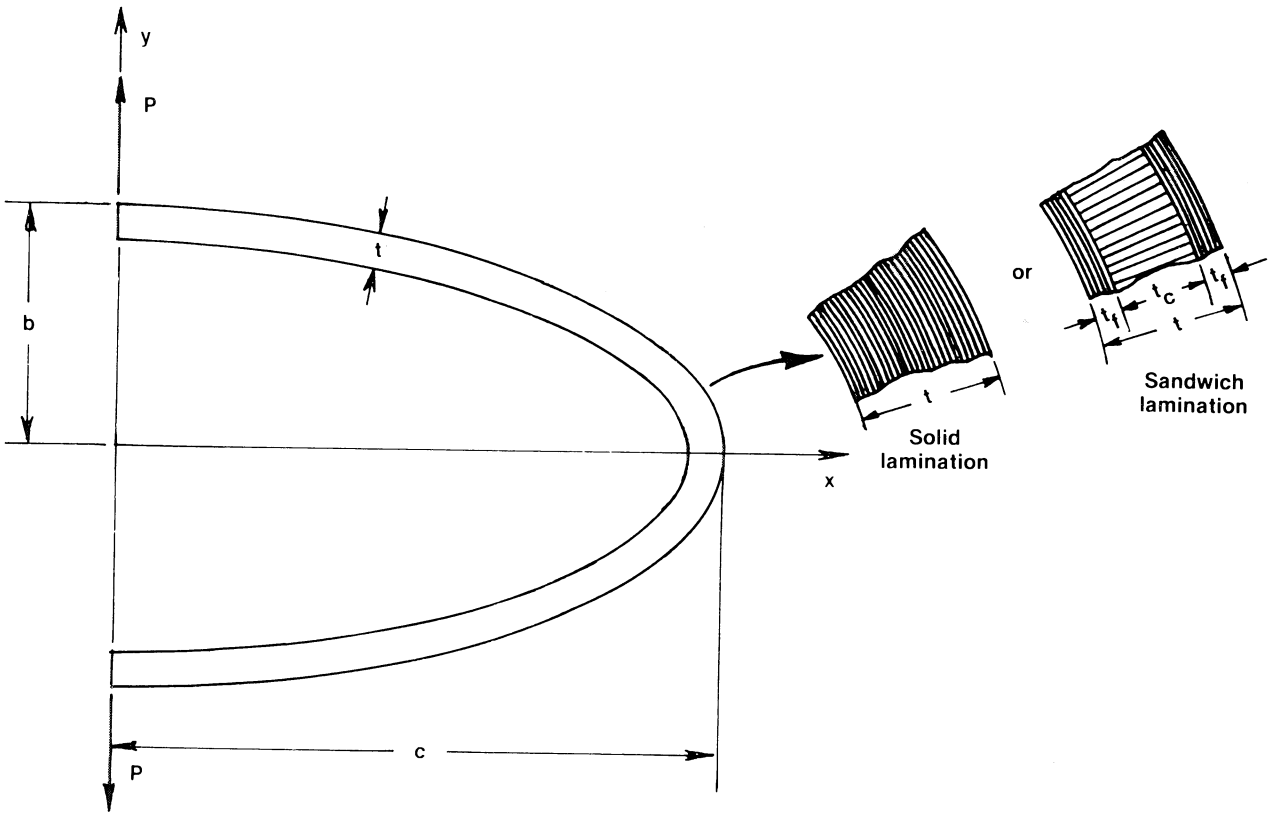

Figure 4. Elliptic curved bar under end forces.

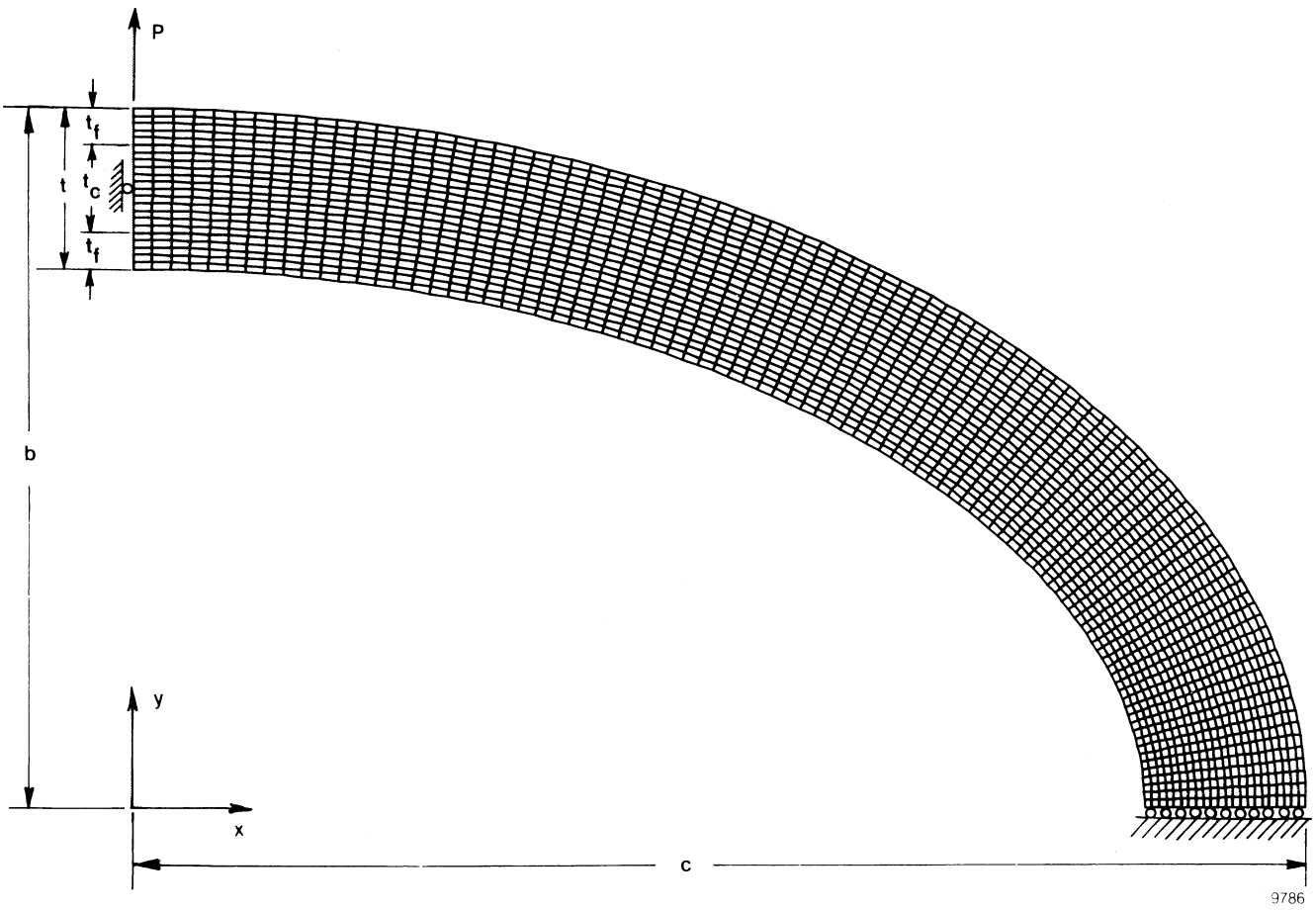

Figure 5. Finite element model for multilayered elliptic curved bar; $b/c = 0.6$.

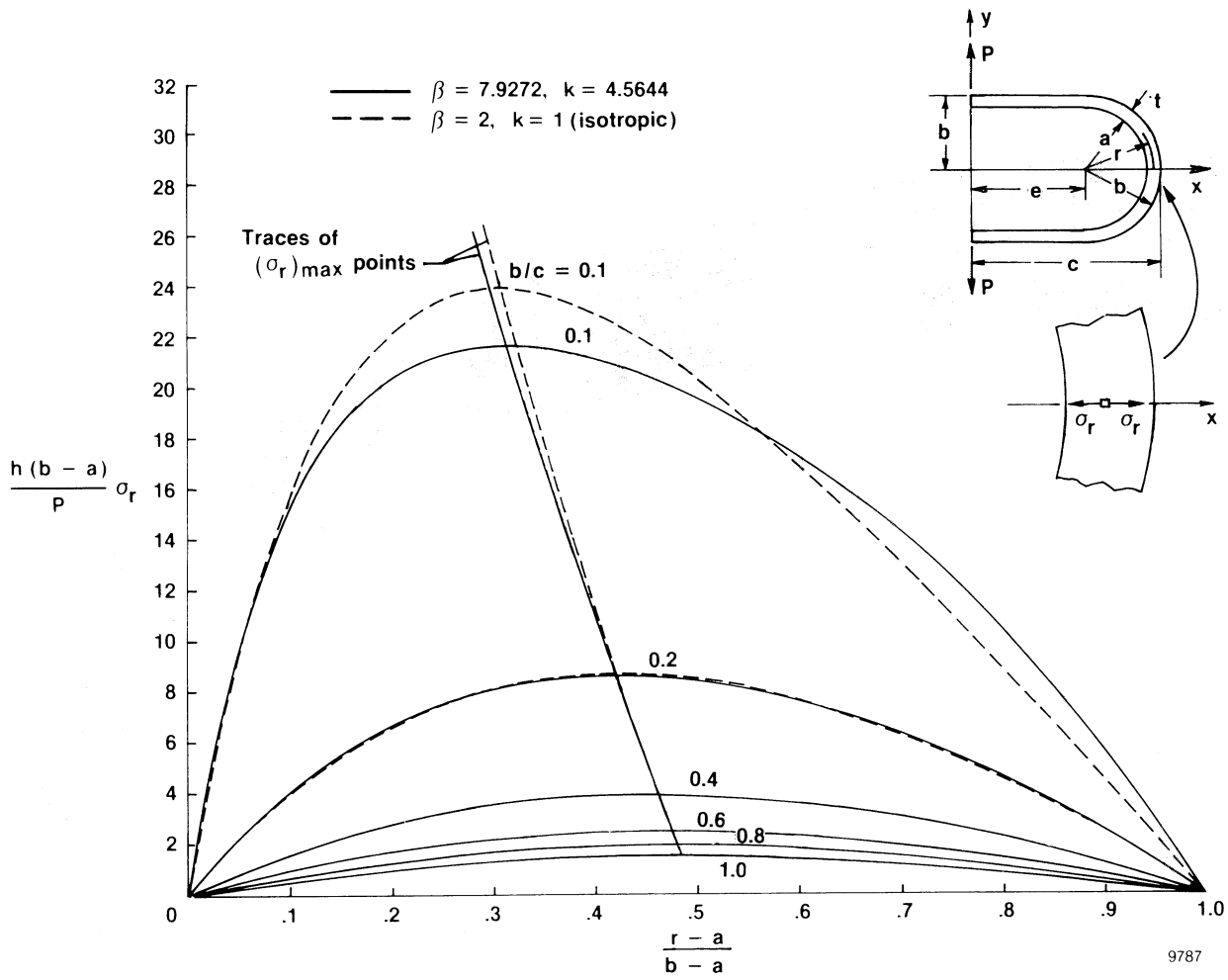

Figure 6. Distributions of radial stress σ_r along x-axis in horseshoe curved bars with different aspect ratios.

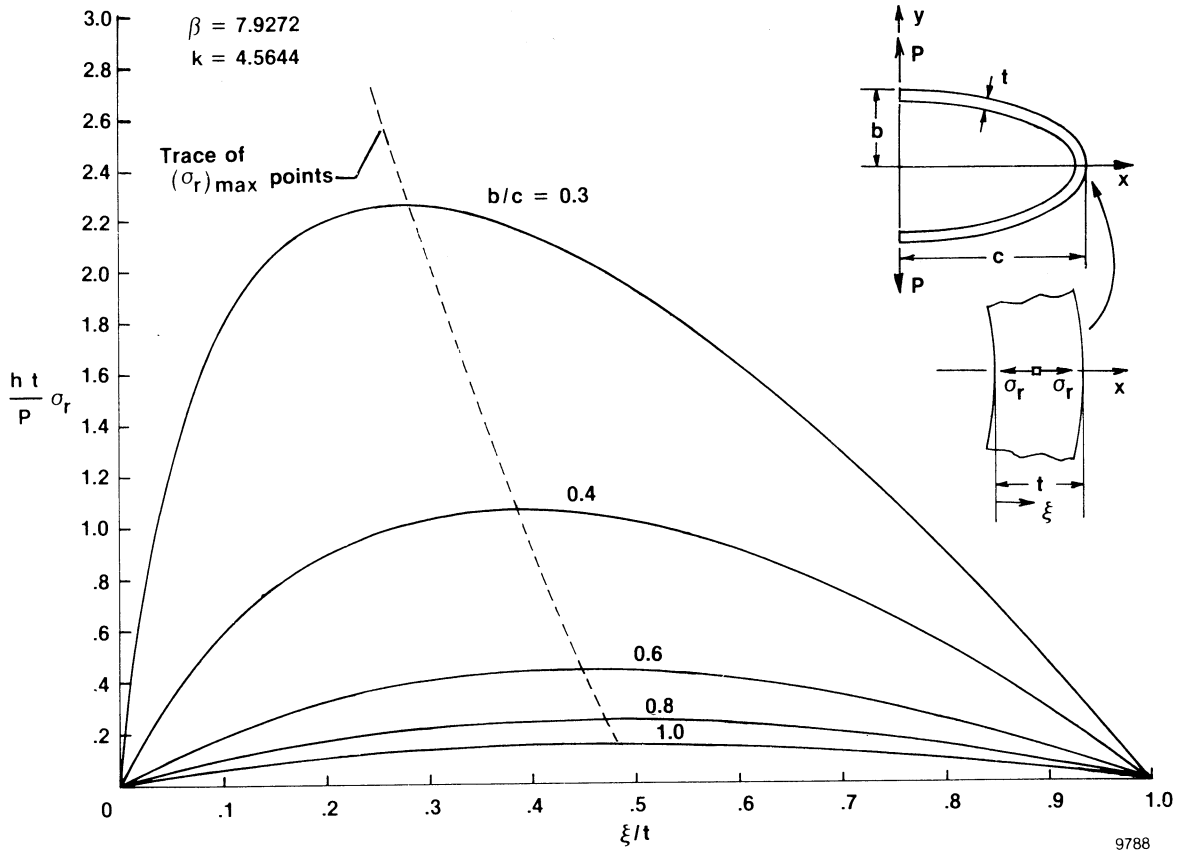

Figure 7. Distributions of radial stress σ_r along x-axis in elliptic curved bars with different aspect ratios.

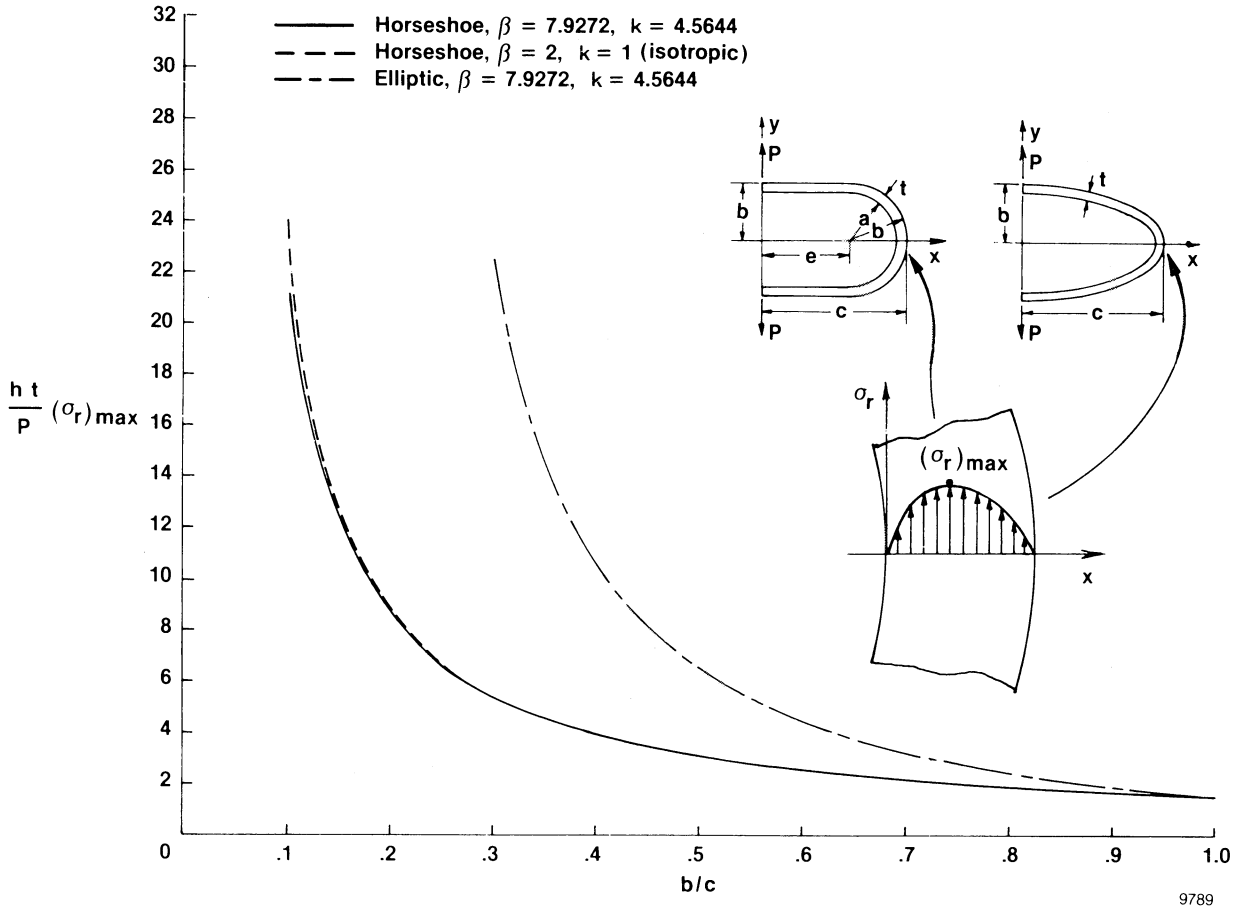

Figure 8. Open-mode delamination stresses in curved bars as functions of aspect ratio.

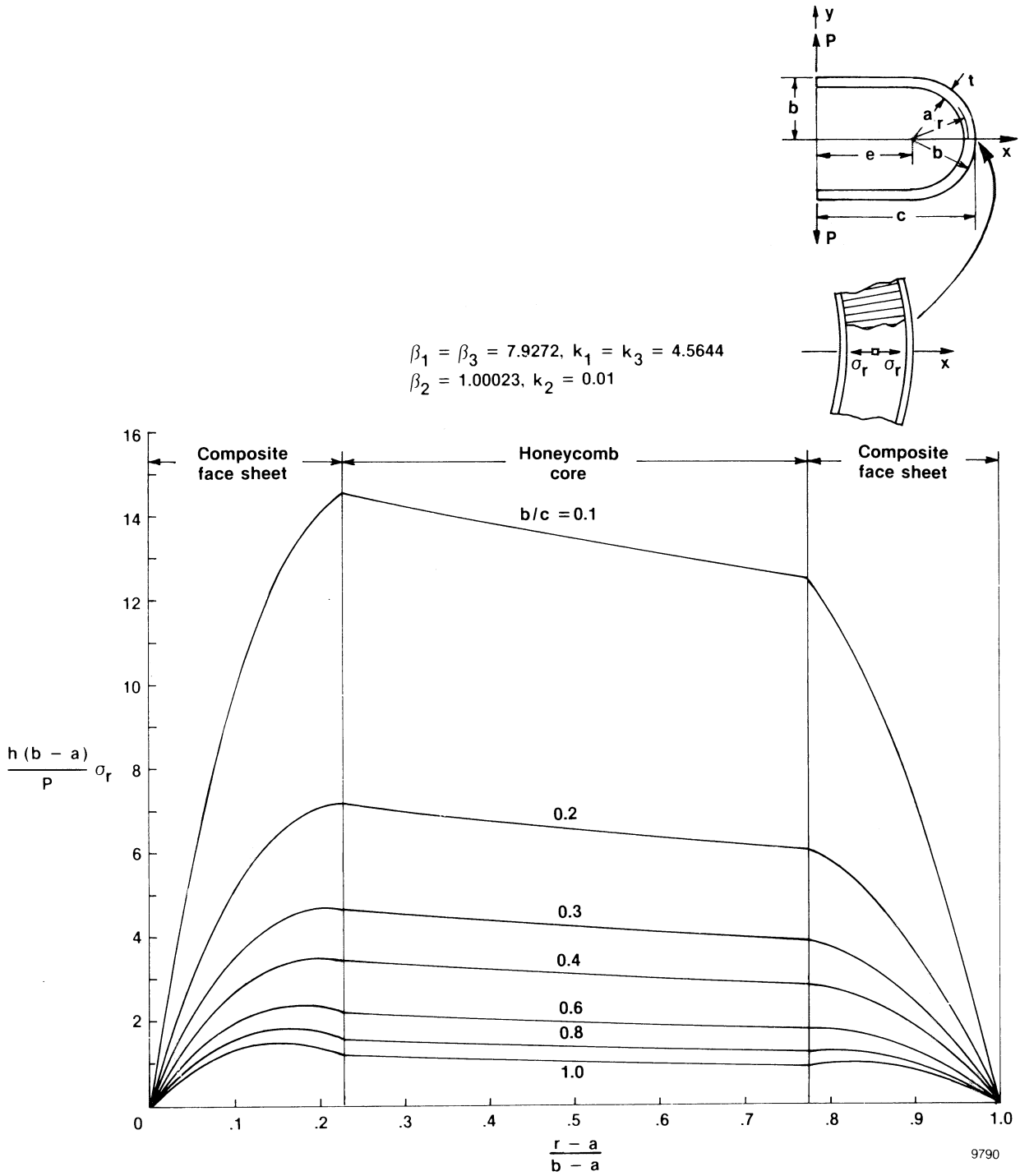

Figure 9. Distributions of radial stress along x-axis in horseshoe sandwich curved bars with different aspect ratios.

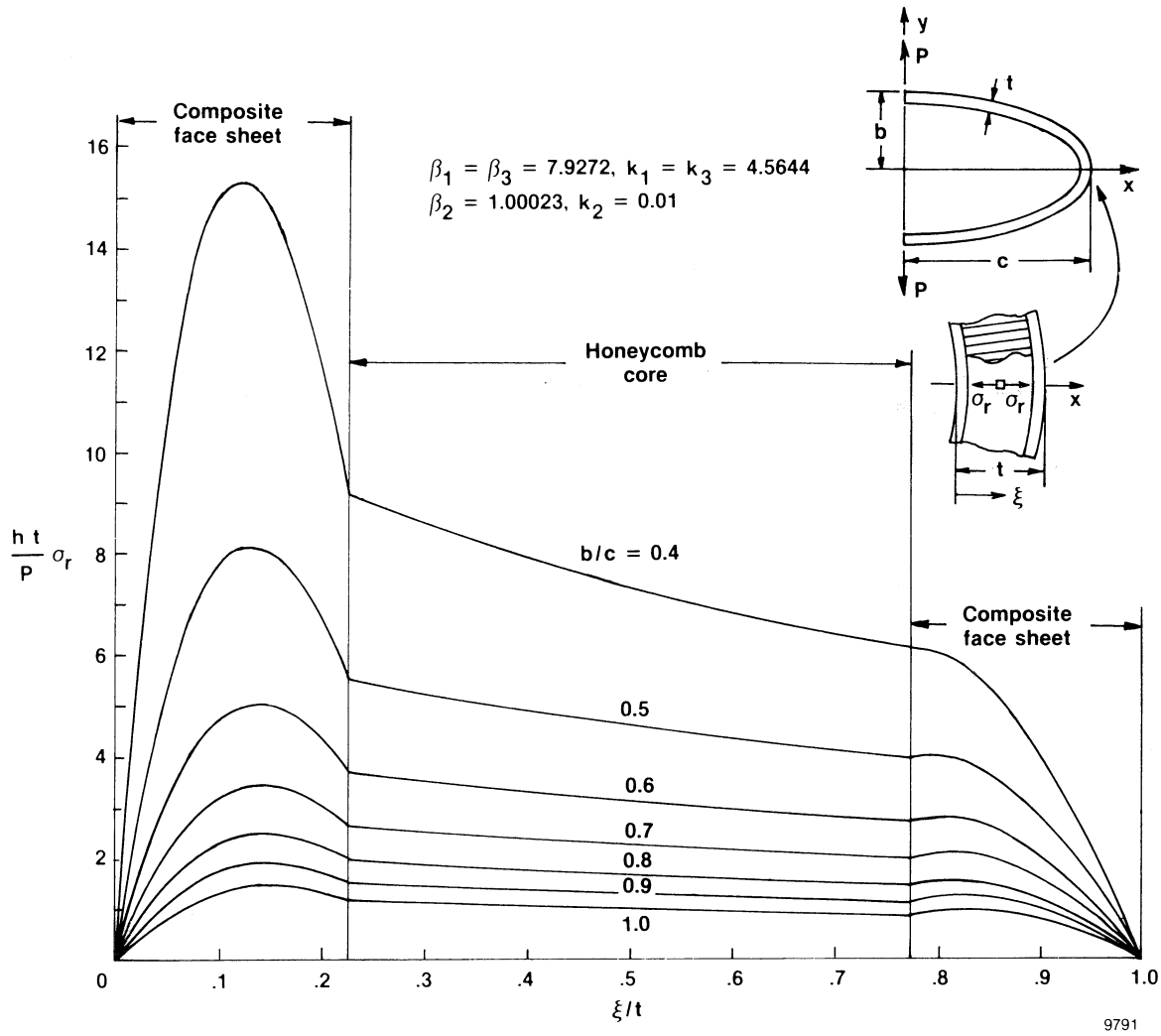

Figure 10. Distributions of radial stress along x-axis in elliptic sandwich curved bars with different aspect ratios.

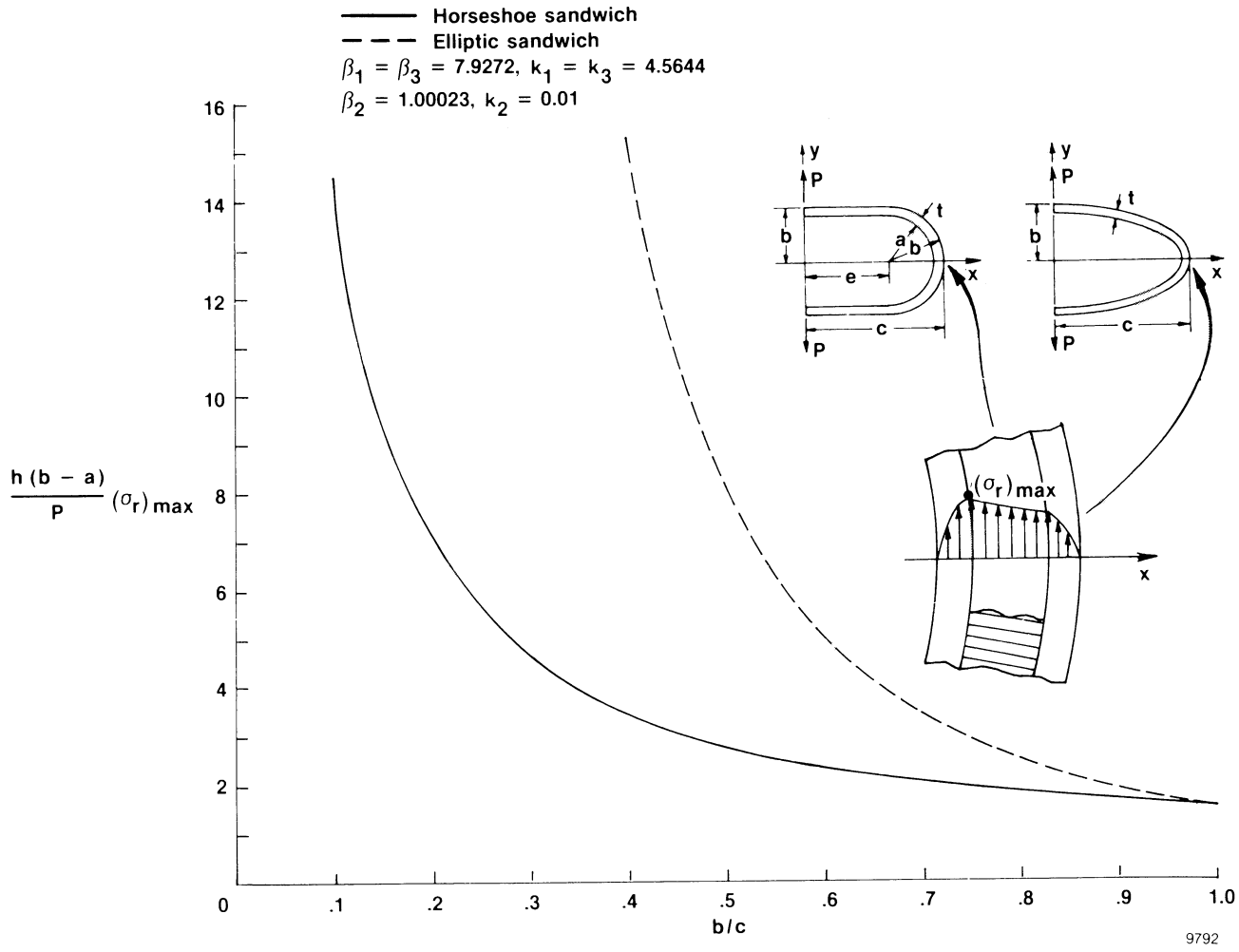

Figure 11. Open-mode delamination stress in horseshoe sandwich curved bar as a function of aspect ratio.

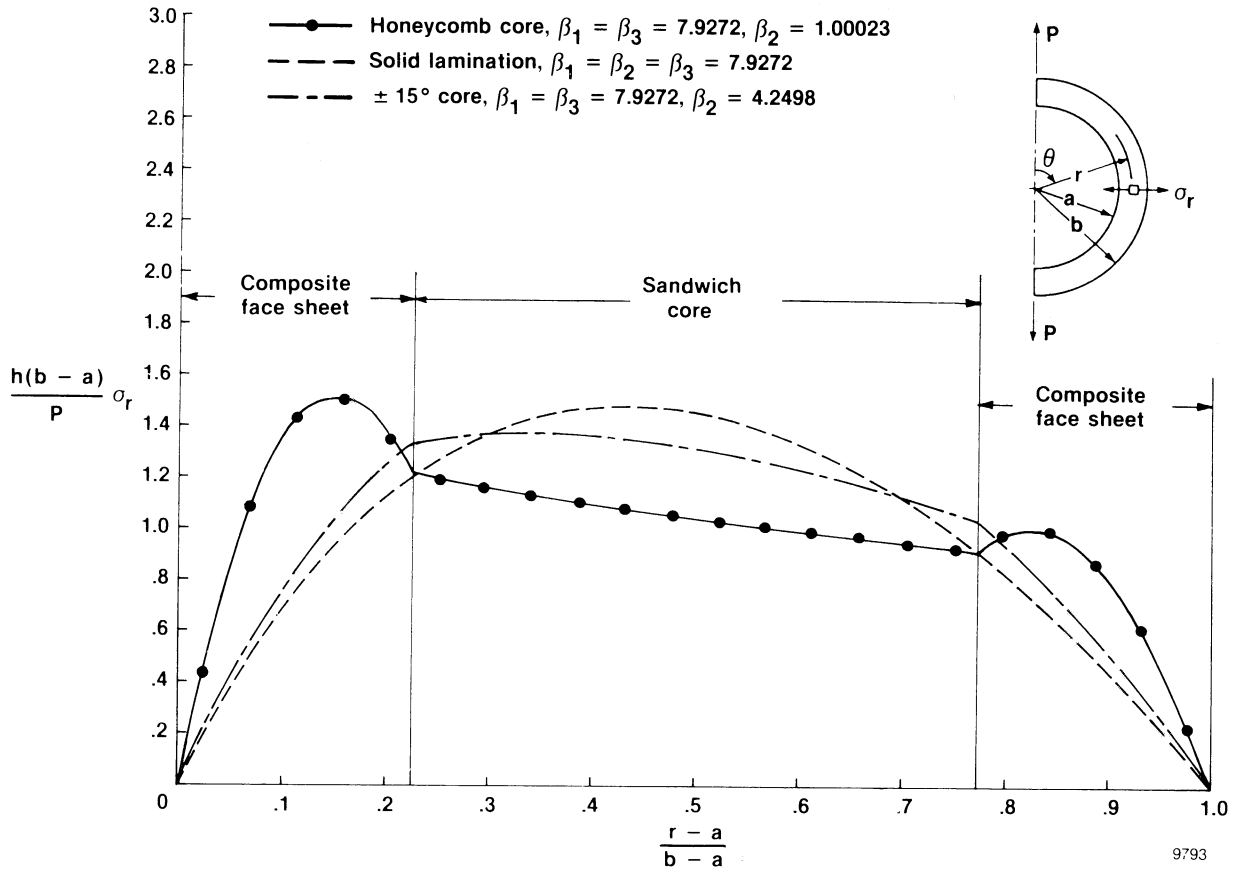

Figure 12. Distributions of radial stress in $\theta = \pi/2$ plane of a semicircular sandwich curved bar under end forces.

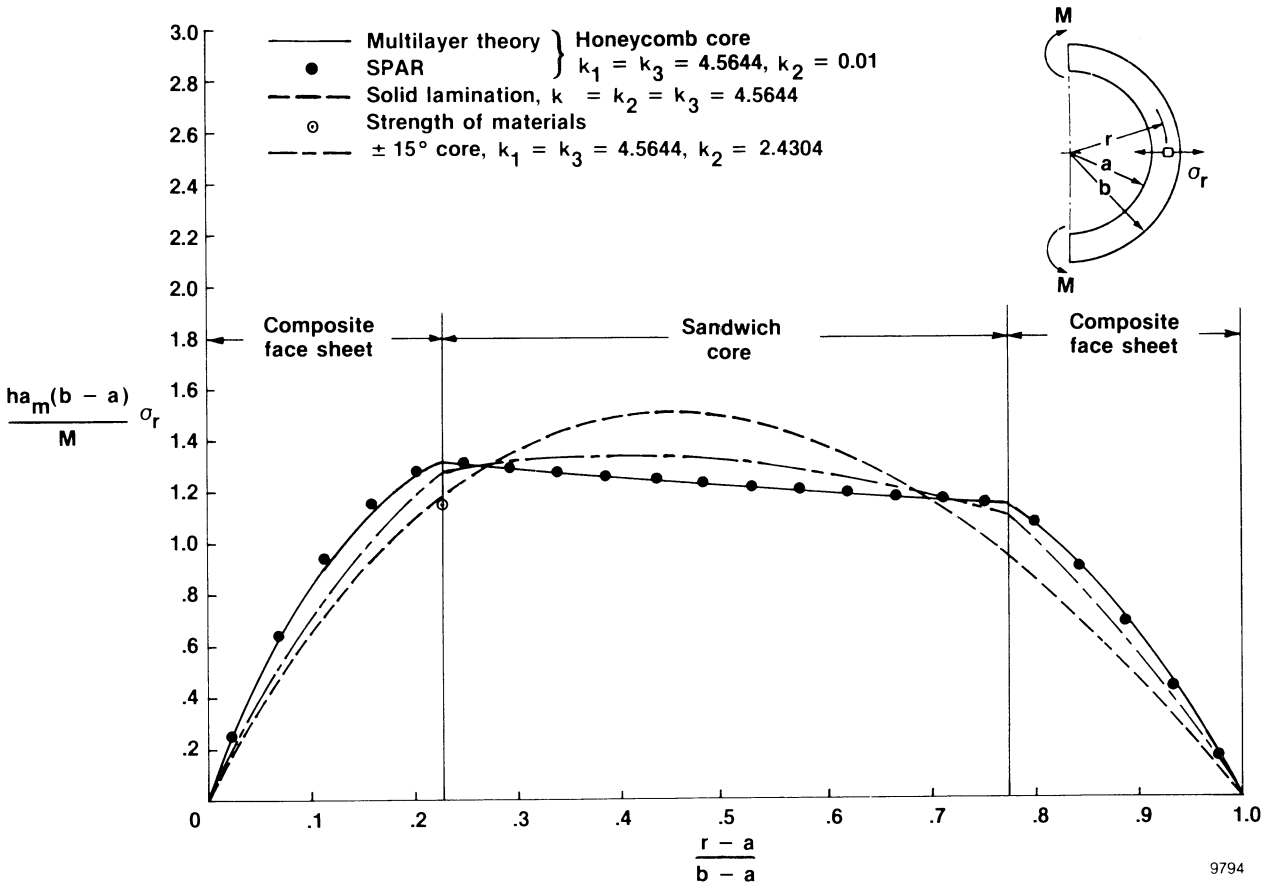

Figure 13. Distributions of radial stress in a semicircular sandwich curved bar under end moments.

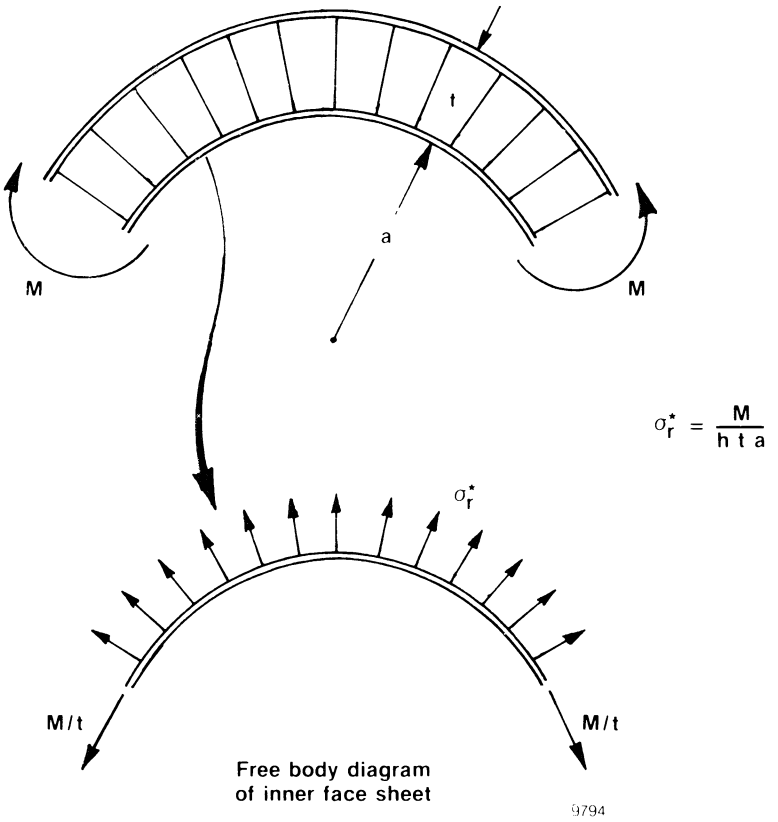

Figure 14. Strength-of-materials debonding stress σ_r^* induced in sandwich curved beam under pure bending.

NASA National Aeronautics and Space Administration

Report Documentation Page

1. Report No.	2. Government Accession No.	3. Recipient's Catalog No.
NASA TM-4164		

4. Title and Subtitle

Open-Mode Delamination Stress Concentrations in Horseshoe and Elliptic Composite Curved Bars Subjected to End Forces

5. Report Date

January 1990

6. Performing Organization Code

7. Author(s)

William L. Ko and Raymond H. Jackson

8. Performing Organization Report No.

H-1567

10. Work Unit No.

RTOP 522-09-01

9. Performing Organization Name and Address

NASA Ames Research Center
Dryden Flight Research Facility
P.O. Box 273, Edwards, California 93523-5000

11. Contract or Grant No.

13. Type of Report and Period Covered

Technical Memorandum

12. Sponsoring Agency Name and Address

National Aeronautics and Space Administration
Washington, DC 20546

14. Sponsoring Agency Code

15. Supplementary Notes

16. Abstract

The multilayer theory of anisotropic elasticity and a finite element method were used to analyze the open-mode delamination stress concentrations in horseshoe and elliptic laminated composite curved bars. Two types of laminations, solid laminations and sandwich laminations, were analyzed.

It was found that the open-mode delamination stress concentration could be greatly increased in these two types of curved bars by decreasing their aspect ratios. The open-mode delamination stress concentration generated in the solid laminations was found to be far more severe than that generated in the sandwich laminations.

The horseshoe curved bar may be used to determine both the open-mode delamination strength of solidly laminated composites and the open-mode debonding strength of sandwiched laminated composites. However, the elliptic curved bar is only good for determining the open-mode delamination strength of solidly laminated composites.

17. Key Words (Suggested by Author(s))

Delamination stresses; Elliptic curved bar; Horseshoe curved bar; Laminated composites; Sandwich laminations; Solid laminations

18. Distribution Statement

Unclassified — Unlimited

Subject category 24

19. Security Classif. (of this report)	20. Security Classif. (of this page)	21. No. of pages	22. Price
Unclassified	Unclassified	25	A02

NASA FORM 1626 OCT 86

**For sale by the National Technical Information Service, Springfield, VA 22161-2171.*

NASA-Langley, 1990